

AD-A152 013

VISCOUS EFFECTS ON BLAST WAVE FLOWFIELDS(U) ACUREX
CORP/AEROTHERM MOUNTAIN VIEW CA B C BENNETT ET AL
DEC 84 FR-85-11/ATD ARO-18104.1-EG DAAG29-81-C-0018

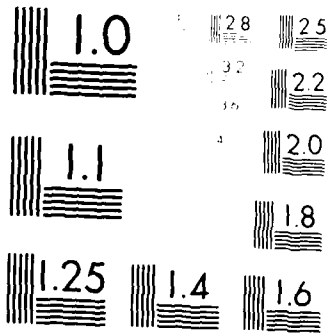
1/1

UNCLASSIFIED

F/G 20/4

NL

								END					
								FILED					
								etc					



MICROCOPY RESOLUTION TEST CHART
NBS 1963-A

AD-A152 013

VISCOUS EFFECTS ON BLAST WAVE FLOWFIELDS

Acurex Final Report FR-85-11/ATD

B. C. Bennett, M. J. Abbett, C. J. Wolf

December 1984

U.S. Army Research Office

Contract No. DAAG29-81-C-0030

Acurex Corporation
Aerotherm Division
555 Clyde Avenue
P.O. Box 7555
Mountain View, California 94039

DTIC
ELECTRONIC
MAR 29 1985
S D

DTIC FILE COPY

The view, opinions, and/or findings contained in this report are those of the authors and should not be construed as an official department of the Army position, policy, or decision, unless so designated by other documentation.

Approved for public release; distribution unlimited.

UNCLASSIFIED

SECURITY CLASSIFICATION OF THIS PAGE (When Data Entered)

REPORT DOCUMENTATION PAGE		READ INSTRUCTIONS BEFORE COMPLETING FORM	
1. REPORT NUMBER ARO 18104.1-EG	2. GOVT ACCESSION NO. AD-A152015	3. RECIPIENT'S CATALOG NUMBER N/A	
4. TITLE (and Subtitle) Viscous Effects on Blast Wave Flowfields		5. TYPE OF REPORT & PERIOD COVERED 1 Jul 81 - 31 Aug 84 Final Report	
		6. PERFORMING ORG. REPORT NUMBER	
7. AUTHOR(s) B. C. Bennett, M. J. Abbett, C. J. Wolf		8. CONTRACT OR GRANT NUMBER(s) DAAG29-81-C-0030	
9. PERFORMING ORGANIZATION NAME AND ADDRESS Acurex Corporation		10. PROGRAM ELEMENT, PROJECT, TASK AREA & WORK UNIT NUMBERS	
11. CONTROLLING OFFICE NAME AND ADDRESS U. S. Army Research Office Post Office Box 12211 Research Triangle Park, NC 27709		12. REPORT DATE Dec 84	
		13. NUMBER OF PAGES 41	
14. MONITORING AGENCY NAME & ADDRESS (if different from Controlling Office)		15. SECURITY CLASS. (of this report) Unclassified	
		15a. DECLASSIFICATION/DOWNGRADING SCHEDULE	
16. DISTRIBUTION STATEMENT (of this Report) Approved for public release; distribution unlimited.		Accession For <input checked="" type="checkbox"/> DTIC <input type="checkbox"/> GPO <input type="checkbox"/> NTIS <input type="checkbox"/> Unannounced <input type="checkbox"/> Justification	
17. DISTRIBUTION STATEMENT (of the abstract entered in Block 20, if different from Report) NA		By Distribution/ Availability Codes Avail and/or Dist Special	
18. SUPPLEMENTARY NOTES The view, opinions, and/or findings contained in this report are those of the author(s) and should not be construed as an official Department of the Army position, policy, or decision, unless so designated by other documentation.		A-1	
19. KEY WORDS (Continue on reverse side if necessary and identify by block number) Viscous Flow Turbulence Flow Fields Structures Blast Waves Shock Waves Flow Separation			
20. ABSTRACT (Continue on reverse side if necessary and identify by block number) The flow resulting from the interaction of a planar shock wave and an object on the ground was calculated with the full Navier-Stokes equations, including turbulence effects. The resulting flowfields show the development of regions of separation both before and aft of the structure, thus illustrating the importance of including turbulence and viscous effects in predicting flowfields resulting from blast waves passing over structures.			

VISCOUS EFFECTS ON BLAST WAVE FLOWFIELDS

Acurex Final Report FR-85-11/ATD

B. C. Bennett, M. J. Abbett, C. J. Wolf

December 1984

U. S. Army Research Office

Contract No. DAAG29-81-C-0030

Acurex Corporation
Aerotherm Division
555 Clyde Avenue
P.O. Box 7555
Mountain View, California 94039

TABLE OF CONTENTS

<u>Section</u>		<u>Page</u>
1	INTRODUCTION AND OVERVIEW	1
2	ANALYSIS	4
	2.1 Governing Equations	4
	2.2 Numerical Algorithm	6
	2.3 Boundary and Initial Conditions	7
	2.4 Time Accuracy	9
3	TEST CASES	10
	3.1 Boundary Layer Development Behind a Shock Wave	10
	3.1.1 Grids	12
	3.1.2 Laminar Results	14
	3.1.3 Turbulent Results	17
	3.2 Shock-Cylinder Interaction	20
	3.2.1 Results	22
4	SHOCK STRUCTURE FLOWFIELD	30
	4.1 Problem Description	30
	4.2 Grid	31
	4.3 Results	31
5	SUMMARY AND CONCLUSIONS	38
	REFERENCES	40

LIST OF ILLUSTRATIONS

Figure		<u>Page</u>
1-1	Schematic of blast wave flowfield interacting with a field vehicle	2
2-1	Generalized curvilinear coordinate transformation	6
2-2	Schematic of initial conditions for blast wave flow problem	7
3-1	Schematic of boundary layer behind shock	11
3-2	Portion of rectilinear grid used in laminar flow behind a shock calculation	12
3-3	Mach number isopleths for laminar boundary layer on flat plate behind shock	15
3-4	Laminar velocity profiles in shock frame of reference	16
3-5	Friction coefficient as a function of nondimensional distance behind the shock for a laminar boundary layer behind shock	16
3-6	Mach number isopleths for turbulent boundary layer on flat plate behind shock	18
3-7	Grids used in shock-cylinder interaction calculations	21
3-8	Pressure-time histories for shock-cylinder interaction	23
3-9	Computed inviscid isopycnics of shock-cylinder interaction at various times	24
3-10	Computed turbulent-viscous isopycnics of shock-cylinder interaction at various times	25
3-11	Development of separation bubble behind cylinder in turbulent viscous flow of shock-cylinder interaction calculation	28
3-12	Calculated inviscid stream function contours of shock cylinder interaction at 4.2 ms	29
4-1	Grid used for shock field structure flow	32

LIST OF ILLUSTRATIONS (concluded)

<u>Figure</u>		<u>Page</u>
4-2	Calculated pressure-time histories for shock-field structure interaction	34
4-3	Computed turbulent-viscous isopycnics of shock-field structure interaction at various times	35
4-4	Stream function contours showing development of separated flow at rear of structure	36
4-5	Stream function contours showing development of separated flow in front of structure	37

LIST OF TABLES

<u>Table</u>		<u>Page</u>
3-1	Grid parameters	13
3-2	Flow parameters	15
3-3	Comparison of results with experimental data for turbulent flow behind a moving shock wave	19

SECTION 1
INTRODUCTION AND OVERVIEW

The objective of this research is to evaluate the effects of viscous and turbulence phenomena on the flowfield behind a blast wave which passes over a structure. Viscous effects have not been previously considered in evaluating such phenomena. However, it is well known that viscosity has global effects on steady flows, such as being the mechanism that leads to flow separation. Therefore, it is quite likely that the predicted blast wave loading on a structure is affected by viscous forces in the flowfield and that it is important to include these effects in comparisons with laboratory data. Moreover, there is a need for flowfield predictions that resolve boundary and shear layers because other effects, such as dust lofting and transport, are influenced by these details of the flow.

It is useful to divide the interaction time into two primary regimes, early and late time. We will use early time to refer to the interval during which and immediately after the blast wave passes over the structure. The late time period corresponds to the time when the shock front is far from the object (compared to typical dimensions of the structure).

The highest impulsive loads occur during the early time regime. The viscous layers are generally quite thin, and the flowfield is primarily inviscid. However, depending on the configuration and flow conditions, the viscous layer might separate, resulting in a radically different flowfield

structure, as illustrated in Figure 1-1, which shows a schematic of a blast wave flowfield passing over a vehicle. The asymmetric pressure loads have resultant forces and moments which may damage the vehicle, move it laterally, or turn it over. The resulting motion or damage varies depending on the history of the developing flowfield, including whether or not the flow separates.

Data show that the rate at which a flowfield can change from attached to separated flow scales with the Strouhal number, $S_t = u/\lambda$, where u is the mean stream flow velocity, λ is a typical length of the structure, and τ is the time interval.¹ For impulsive flowfield changes, $S_t = 0.17$. For a 5 psi overpressure blast wave, with $\lambda = 10$ ft, this gives $\tau = 0(10^{-3})$ s. For a typical vehicle under these conditions, the angular rotation rate due to the large, asymmetric side loads is roughly $10^\circ/\text{s}$. Thus, the vehicle response time is on the order of 0.1 to 10 s, and it is clear that separation can occur quickly enough to affect the dynamics of forces and moments on vehicles and structures.

During the late time period, the flowfield structure changes more gradually. Thick viscous layers develop, becoming comparable to or larger than the height of typical structures. The turbulence flow may loft

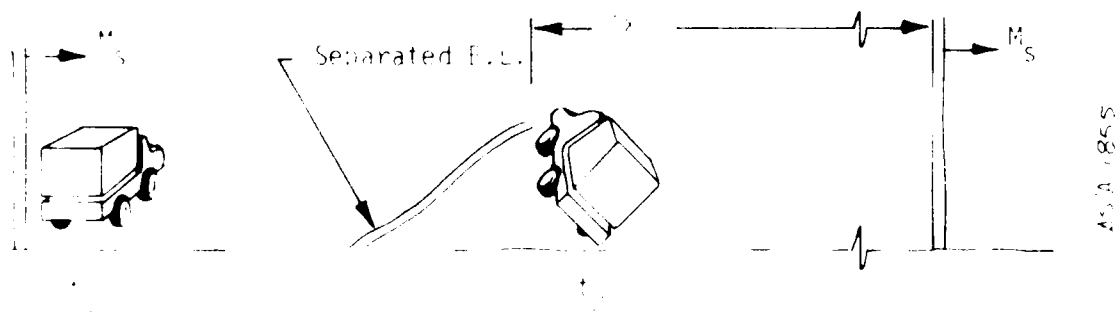


Figure 1-1. Schematic of blast wave flowfield interacting with a field vehicle.

considerable debris (pebbles, rocks, dirt, etc.) into the flowfield, thereby interfering with communications and possibly damaging structural components.

Recently, the U.S. Army Ballistic Research Laboratory supported research by Kutler and Fernquist² on the inviscid flowfield associated with blast wave-structure interactions. The present study extends this earlier work to include viscous/turbulence effects. We have used the same kinds of finite difference methods, solution procedures, and computer codes as Kutler and Fernquist. We studied first the simple viscous flow in a shock tube, which serves to validate the treatment of the viscous terms in the equation of motion. These results compare well with shock tube data and "exact" boundary layer theory for this case. We have also made both viscous and inviscid calculations for a blast wave flow over a free-standing cylinder and for a half cylinder resting on a flat surface. The present results for a free-standing cylinder compare quite well with previous results and data. The flow over a half cylinder plate is a prototype of the geometry of a common installation (e.g., building, vehicle), which is an object on the earth's surface. It includes the additional feature of the boundary layer development associated with the incoming flow, which appears to be the cause of an upstream separated flow region. This result appears to be a unique phenomena not likely to be of practical interest.

This report is organized in four parts. Section 2 describes the governing equations, numerical algorithm, and the boundary conditions used. Section 3 describes the test cases and their results. The flow behind a shock wave, flow over a plate, and the interaction of a shock and a cylinder are described in order of increasing difficulty. Section 4 explains the results of our analysis of the interaction between a shock wave and an object on the ground. Finally, section 5 concludes and summarizes the report.

SECTION 2

ANALYSIS

The physical problem of interest is the interaction of blast waves with objects protruding from a surface as shown in Figure 1-1. However, as a shock moves along a surface, a boundary layer develops behind it and shear forces change the flowfield. Therefore, to adequately describe this flow the compressible mean Navier-Stokes equations in two dimensions (2-D) are employed. In this study, relatively weak blast waves are considered and the time frame of the calculation is relatively short. Therefore, the blast wave is approximated as a constant speed shock wave. In addition, the gas is assumed to be thermally and calorically ideal.

2.1 GOVERNING EQUATIONS

The Navier-Stokes equations in Cartesian coordinates for two-dimensional flow can be written in dimensionless, conservative-law form for a perfect gas without external forces as follows:²

$$\rho_t + \partial_x E + \partial_y F = Re^{-1} (\partial_x E_v + \partial_y F_v) \quad (2-1)$$

where

$$\rho = \begin{bmatrix} \rho \\ \rho u \\ \rho v \\ e \end{bmatrix}, \quad E = \begin{bmatrix} \rho u \\ \rho u^2 + p \\ \rho uv \\ u(e + p) \end{bmatrix}, \quad F = \begin{bmatrix} \rho v \\ \rho uv \\ \rho v^2 + p \\ v(e + p) \end{bmatrix}, \quad (2-2)$$

$$F_V = \begin{bmatrix} 0 \\ \tau_{xx} \\ \tau_{xy} \\ f_4 \end{bmatrix}, \quad F_V = \begin{bmatrix} 0 \\ \tau_{xy} \\ \tau_{yy} \\ g_4 \end{bmatrix} \quad (2-2)$$

with

$$\begin{aligned} \tau_{xx} &= \mu(4u_x - 2v_y)/3 \\ \tau_{xy} &= \mu(v_y - u_x) \\ \tau_{yy} &= \mu(-2u_x + 4v_y)/3 \\ f_4 &= \mu r_{xx} + \nu \tau_{xy} + \mu \rho r^{-1}(\gamma - 1)^{-1} \partial_x a^2 \\ g_4 &= \mu \tau_{xy} + \nu \tau_{yy} + \mu \rho r^{-1}(\gamma - 1)^{-1} \partial_y a^2 \end{aligned} \quad (2-3)$$

In the above equations, the density ρ is nondimensionalized by ρ_∞ , the velocity components u and v in the x and y directions by a_∞ , and the total energy e by $\rho_\infty a_\infty^2$. Assuming a reference length, ℓ , the time is nondimensionalized by ℓ/a_∞ , the dynamic viscosity μ by μ_∞ , the pressure p by $\rho_\infty a_\infty^2$. Pressure is related to the conservative flow variables by the equation of state:

$$p = (\gamma - 1) e - \frac{1}{2} \rho (u^2 + v^2) \quad (2-4)$$

To transform equation (2-1) for mapping complicated physical space into rectangular computational space (see Figure 2-1) the following independent variable transformation is chosen:

$$\begin{aligned} x &= x^* \\ y &= y^* \\ t &= t^* \\ \tau &= \tau^* \end{aligned} \quad (2-5)$$

Figure 2. Comparison of results with experimental data for turbulent flow behind a moving shock wave.

Investigator	M_S	Re_{λ_S}	C_f	$St \cdot RE^{1/5}$
<u>Experimental</u>				
Martin ¹²	1.53	2.13×10^7	1.35×10^{-3}	
Martin ¹²	1.53	2.50×10^7	1.73×10^{-3}	
Martin ¹²	1.53	3.40×10^7	1.68×10^{-3}	
Martin ¹³	1.54	--	--	3.54×10^{-2}
Martin ¹⁴	2.41	--	--	3.85×10^{-2}
Martin ¹⁵	1.47	--	--	3.50×10^{-2}
Martin ¹⁶	2.61	--	--	4.41×10^{-2}
Present study	1.53	5.40×10^7	1.54×10^{-3}	3.42×10^{-2}
Present study	1.53	4.13×10^7	1.57×10^{-3}	3.05×10^{-2}
Present study	1.53	2.95×10^7	1.61×10^{-3}	1.43×10^{-2}
Present study	1.53	2.96×10^7	1.855×10^{-2}	3.26×10^{-2}

relation to mesh spacing. At a distance of 1m behind the shock this puts several points in the viscous sublayer.

The Mach contours of the turbulent boundary layer behind the moving shock are shown in Figure 3-6, with the outer contour qualitatively representing the edge of the boundary layer. The turbulent boundary layer is thinner but has the same general shape as its laminar counterpart.

The quality of the boundary layer solution is illustrated comparing the local coefficient of friction and Stanton number with measured values. The local coefficient for different Reynold's numbers and values measured by Martini¹² are listed in Table 3-3. The calculated values agree quite well with the experimental data and show the proper trend. Hartunian measured turbulent heat transfer in shock tubes at different conditions and suggests the correlation $St \cdot Re_p^{1/5} = 3.7 \times 10^{-2}$. In this study most of the calculated values are between 3.0×10^{-2} and 3.42×10^{-2} , as listed in Table 3-3.

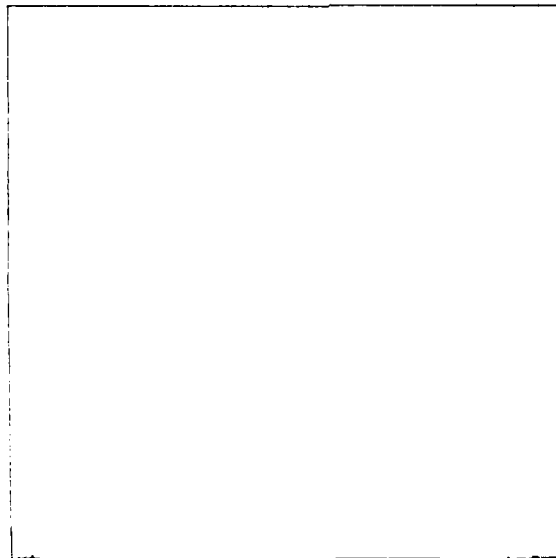


Figure 3-6. Mach number isopleths for turbulent boundary layer on flat plate behind shock

Model's simplicity solution. Good agreement is shown except near the shock. The poor quality of the solution near the shock is expected because the implicit finite difference algorithm of ARC2D (with fourth order dissipation) does not cater to this characteristics for other users. Some effort has been given to eliminating this problem.¹¹ One preliminary solution, the addition of second order dissipation near the shock, has been successful in steady state calculations. Unfortunately, this modification was not available for the present study.

These results demonstrate that the code does a good job of predicting the laminar boundary layer behind a moving shock.

4.1.3 Turbulent Results

The development of a turbulent boundary layer behind a moving shock has also been studied both experimentally and analytically. Hartunian, et al.,¹⁰ measured heat transfer in shock tubes for a wide range of shock strengths. Martin¹² made measurements at only two pressure ratios (2.75 and 8) and compared his results with the approximate turbulent boundary layer theory of Michel.⁹

The turbulent boundary layer studied here is created by a shock with a pressure ratio of 2.75 moving along a flat wall, as was the case for the laminar study. The pressure ratio of 2.75 is somewhat unique in that the fluid freestream velocity behind the shock in the shock frame of reference is equal to the fluid velocity in the wall (or fixed) frame of reference. A constant wall temperature is assumed, which is confirmed by the measurements of both Martin and Hartunian for shocks of this strength. Compared to the laminar flow calculation, much smaller time steps were used for turbulent flow because there is finer mesh spacing at the wall. The grid spacing at the wall of 10^{-5} m, required to obtain results that are independent of further

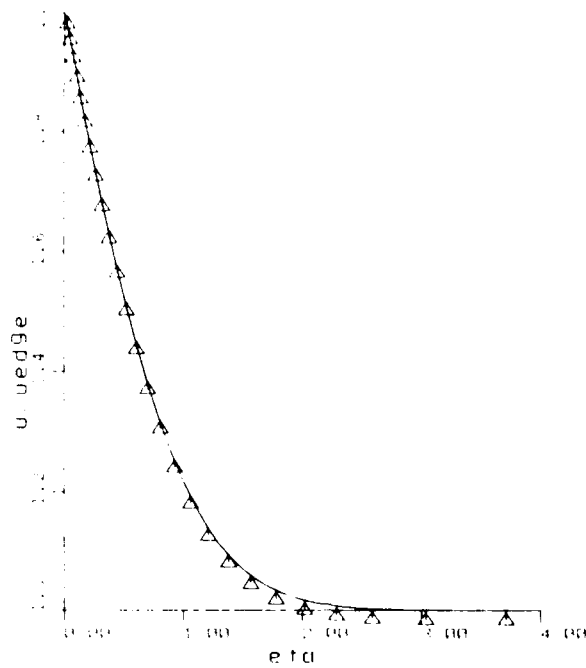


Figure 3-4. Laminar velocity profiles in shock frame of reference (Symbols represent calculated values, line represents Mirels' self similar solution)

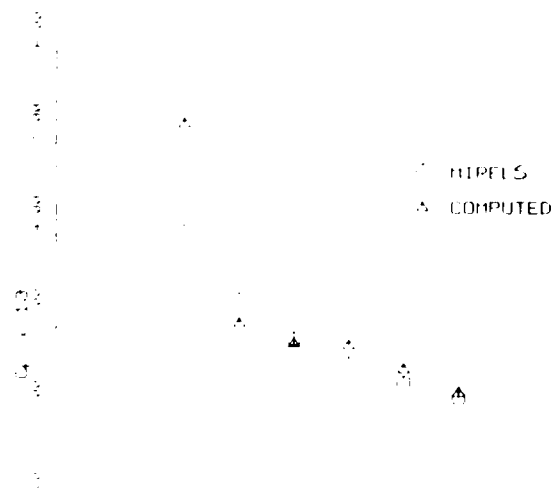


Figure 3-5. Friction coefficient as a function of nondimensional distance behind the shock for a laminar boundary layer behind shock

Table 3-2. Flow parameters

Structure	Shock Mach Number	Flow Mach Number	Wall Condition	Type of Flow	Nondimensional Step Size ($t \cdot a_\infty / x$)	Number of Time Steps
Flat wall	1.58	0.673	Adiabatic	Laminar	7.56×10^{-3}	600
Flat wall	1.58	0.673	$T_w/T_\infty = 0.73$	Turbulent	2.5×10^{-3}	1,200
Cylinder	1.16	0.247	Adiabatic	Inviscid	3×10^{-3}	1,720
Cylinder	1.16	0.247	$T_w/T_\infty = 0.90$	Turbulent	4×10^{-5}	140,000
half cylinder on wall	1.58	0.673	$T_w/T_\infty = 0.73$	Turbulent	1.8×10^{-4}	23,000

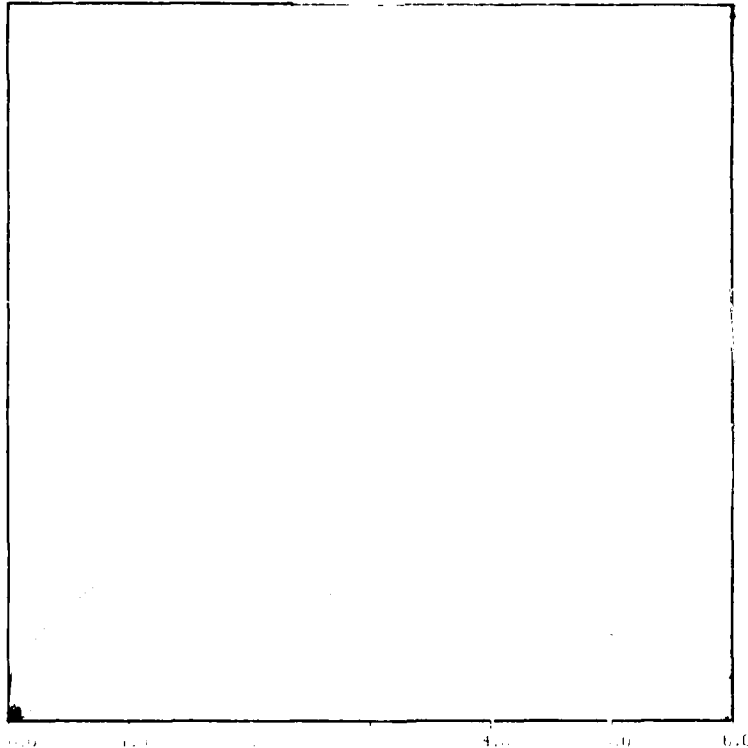


Figure 3-3. Mach number isopleths for laminar boundary layer on flat plate behind shock

3.1.2 Laminar Results

Our predictions of a laminar boundary layer are compared to the "analytic" results of Mirels in this section. We will follow Mirels' transformation of the unsteady problem of a shock wave moving over a wall to that of a steady flow by presenting our results in the shock fixed frame of reference. Mirels used the Prandtl boundary layer equations and applied a similarity variable which is a function of the freestream velocity, fluid parameters, and distance behind the shock. The resulting equation is an ordinary differential equation which Mirels integrated numerically. Hartunian, et al.,¹⁰ found good agreement between their measured heat transfer rates and those calculated with the equations derived by Mirels. They also showed that the effects of density and viscosity variations are small for Mach numbers less than 2. These results show Mirels' theory to be a good model for laminar flow.

The laminar flow calculations have a shock Mach number of 1.58. The details of the flow calculation are given in Table 3-2. After 600 steps the shock is 6.2m from the leading edge, and all the results we will show are for this time. Figure 3-3 shows lines of constant Mach number, and qualitatively marks the edge of the boundary layer. It is easy to distinguish the two regions of the flow. Figure 3-4 shows good agreement between the calculated velocity profile with that predicted by Mirels' similarity solutions. In this figure, the ordinate is Mirels' similarity parameter and the velocities are measured relative to the shock. Thus $v/u_e = 2$ is the wall and $u/u_e = 1$ is the freestream. Additionally, throughout the flow the edge velocity normal to the wall, although not shown, has the correct behavior and is directed toward the wall near the shock and away from the wall near the leading edge. Figure 3-5 is a comparison of the computed friction coefficient with that predicted by

Table 3-1. Grid parameters

Grid	Grid Generation	Grid Size	Cylinder Diameter (Reference Length)	Minimum Spacing Normal to Wall	Distance to Outer Boundary	Type of Stretching
Laminar flow behind shock	Analytic	90x45	1	1.1×10^{-4}	14.2	Geometric
Turbulent flow behind shock	Analytic	90x45	1	8×10^{-6}	10.4	Geometric
Inviscid cylinder	Analytic	180x35	1	4×10^{-3}	10	Exponential
Viscous cylinder	Analytic	180x49	1	8×10^{-5}	8	Exponential
Field structure	Hyperbolic	166x65	1	1.75×10^{-4}	8	Exponential

the most suitable test for a calculation of laminar flow behind a shock is a comparison with Mirels' similarity solution.⁹ Mirels' results have been compared favorably with experimental data,¹⁰ and the analysis required to compare to the work is quite straightforward. Comparison with experimental data is more appropriate for turbulent flow.

3.1.1 Grids

The grids used for these calculations are rectilinear. A portion of the grid for the laminar case is shown in Figure 3-2. The grid used for turbulent flow was similar, but with finer spacing at the wall. Both grids use geometric stretching away from the wall and a constant spacing in the streamwise flow (x) direction. The acceptable minimum y spacing (normal to the wall) was determined by reducing the spacing at the wall until the solution was independent of the wall spacing. Details of the grid are given in Table 3-1.

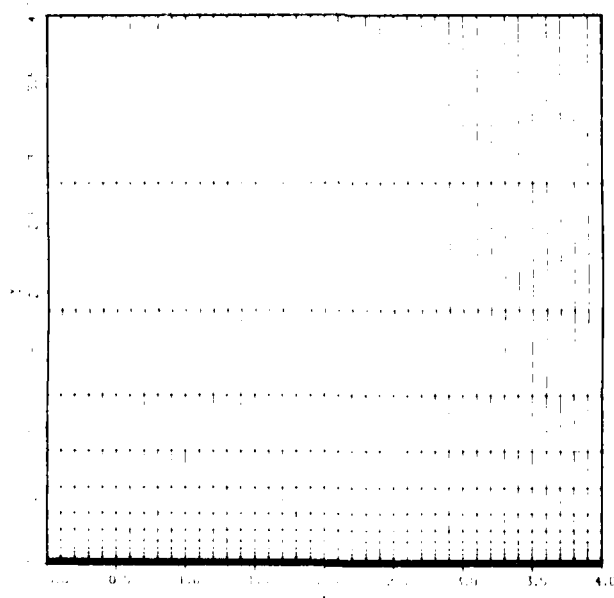


Figure 3-2. Portion of rectilinear grid used in laminar flow behind a shock calculation



Figure 3-1. Schematic of boundary layer behind shock: Region 1 influenced by leading edge, Region 2 influenced by shock

the shock (Region 2). As the shock moves along the wall, both regions grow in length while the thickness of the boundary layer between the two regions increases.

One of the distinct differences between the boundary layer immediately behind the shock and the leading edge type boundary layer is the direction of the fluid velocity normal to the wall. In a boundary layer which grows in the direction of the fluid mean velocity, the fluid must flow away from the wall. In the boundary layer behind a shock the growth is opposite to the direction of the flow and the fluid must move towards the wall for the boundary layer to grow. Hence, the boundary layer edge normal velocity is negative near the shock.

In practice, the laminar part of the boundary layer may be quite short. However, the code ARC2D does not account for transition from laminar to turbulent flow (i.e., computations are either laminar or turbulent). Thus,

SECTION 3

TEST CASES

Although the code ARC2D has been used for a variety of flow problems, there has not been any work with this code on unsteady boundary layer development behind shocks. Therefore, a study was conducted to verify that the results agree with experimental data and relevant analytical results. An additional purpose of the study was to evaluate the grid requirements for these flows. This was done for both laminar and turbulent flows on a flat surface. These results are described in Section 3.1. Calculations were also made for the case of a shock interacting with a cylinder, in both inviscid and viscous flow, as summarized in Section 3.2. The satisfactory results from these studies gives some confidence that this method can successfully be used in applications.

3.1 BOUNDARY LAYER DEVELOPMENT BEHIND A SHOCK WAVE

The development of the boundary layer behind a shock has received considerable attention. Laminar and turbulent flows have been investigated both analytically⁹ and experimentally.¹⁰ The physical problem is illustrated in Figure 3-1. As the shock wave moves along the wall a boundary layer develops behind it. At the same time the boundary layer is developing from the leading edge of the wall.

Thus, the boundary layer has two more or less distinct regions: that influenced by the "leading edge" (Region 1, Figure 3-1) and that influenced by

viscous flows. The body surface pressure is calculated from the normal momentum equation, which is

$$\begin{aligned}
 \rho(\partial_t n_t + u \partial_t n_x + v \partial_t n_y) - \rho U(n_x u_\xi + n_y v_\xi) \\
 &= (n_x \xi_x + \xi_y n_y) p_\xi + (n_x^2 + n_y^2) p_n \\
 &= p_n (n_x^2 + n_y^2)
 \end{aligned}
 \tag{2-6}$$

where n is the local normal to the body surface. Free stream stagnation enthalpy is held constant along the surface for inviscid flows while adiabatic or constant temperature walls are used for viscous flows.

2.4 TIME ACCURACY

Most of the calculations done for this work must be time-accurate.* This means time steps must be limited to a value that makes the Courant number

$$CN = \frac{c \Delta t}{\Delta x}, \text{ where } c \text{ is the velocity in the } x\text{-direction,}$$

less than one. This requirement, the CFL condition, means that as the grid becomes finer, the time step must be reduced. The CFL condition requires that the analytic domain of influence lie within the numerical domain of influence. The maximum CN for all time-accurate calculations for this work is ~ 0.9 .

*That is, we are interested in the transient fluid mechanics, not in obtaining a steady flow as the time-asymptotic limit of a transient flow.

- The region of undisturbed fluid that the shock has not yet reached
- The region behind the shock where the fluid has been affected by the shock moving through it

The computations described here were done with the following initial and boundary conditions.

Initially the flow is set up with two distinct regimes; pre- and postshock, as shown in Figure 2-2. The initial position and Mach number of the shock are input to the program. The entire region in front of the shock is assumed to be undisturbed fluid with no velocity and constant pressure and temperature. Behind the shock the flow conditions are calculated using ideal normal shock relationships. The inflow boundary, \overline{AB} , uses these postshock conditions throughout the calculation. If a wall is adjacent to the inflow boundary, the constant flow profile simulates physically a sharp leading edge condition. At the "outflow" boundary, \overline{CD} , the preshock conditions are applied, and the calculations are stopped before the shock reaches this boundary.

Along the outer boundary, \overline{BC} , either pre- or postshock conditions are applied. The position of the shock is calculated assuming the shock moves at constant velocity of $M_S \cdot a_1$. As one can see, the actual position will most often be between two grid points. In the algorithm used, the grid point behind the shock has postshock conditions, while the grid point in front has preshock conditions. Thus, the shock position on the outer boundary is defined only to within the mesh cell size. This resolution is sufficient for an exploratory study such as this.

Different conditions at solid boundaries were applied depending on the flow. Tangency is satisfied for inviscid flow, while no slip is used for

The turbulence model in ARC2D is a conventional two-layer algebraic mixing length model. The inner layer is governed by the Prandtl mixing length with Van Driest damping. The outer layer follows the Clauser approximation. This turbulence model is detailed by Baldwin and Lomax,⁸ and is appropriate for attached flows. It is probably suspect in separated flows.

For ARC2D to be employed in this shock-interaction work, several changes had to be made to the code. The most important of these pertained to changes in the initial and boundary conditions applied by the code.

2.3 BOUNDARY AND INITIAL CONDITIONS

One aspect of the shock-interaction problem is that the outer boundary conditions are time dependent. As shown in Figure 2-2, there are two distinct flow regimes as the shock moves through the computational domain.

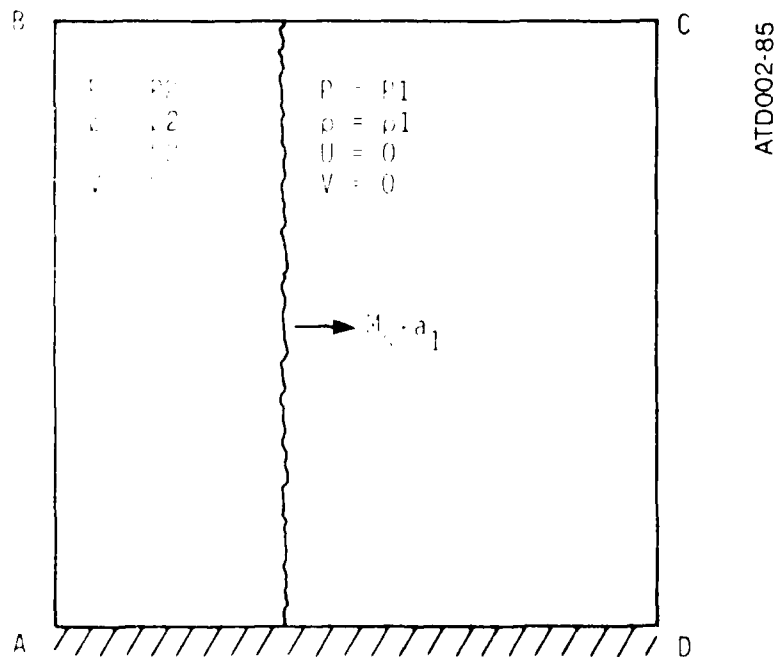
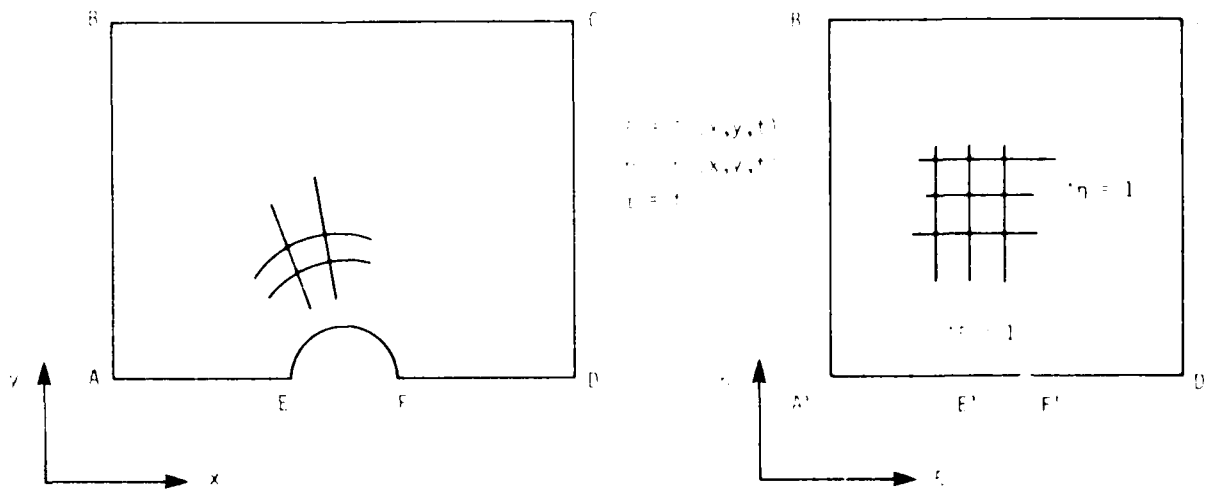


Figure 2-2. Schematic of initial conditions for blast wave flow problem



ATD003-85

Figure 2-1. Generalized curvilinear coordinate transformation

Details of this coordinate transformation are given in the work of Pulliam.³ The transformations are chosen so that the grid spacing in computational space is uniform with unit length. There exists a one-to-one correspondence between a physical point in space and a computational point (except for singularities). With this construction a code can handle a wide variety of physical geometries with boundary-conforming grids.

2.2 NUMERICAL ALGORITHM

The computer program used in this work is a version of the code ARC2D. ARC2D was developed at the NASA Ames Research Center^{3,4} and has been applied to a variety of complex flow problems.^{5,6} ARC2D uses an implicit finite difference numerical algorithm with fourth order dissipation. The algorithm is an implicit approximate factorization scheme which is second order accurate in time. This noniterative scheme is based on the work of Warming and Beam,⁷ and results in easily solved block tridiagonal matrices.

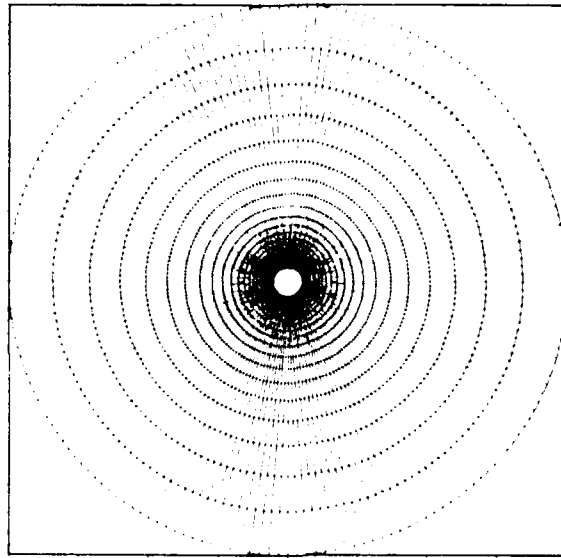
The lowest value listed, 1.4×10^{-7} appears to be due to a numerical oscillation in the solution near the shock. Such oscillations are present in all the calculations and are common to this implicit scheme with fourth order dissipation. Overall this study reveals the method is well suited to capturing the basic character of turbulent-viscous effects behind the shock, although quantitative transfer predictions may require an extremely fine grid near the wall.

3.2.2. SHOCK-CYLINDER INTERACTION

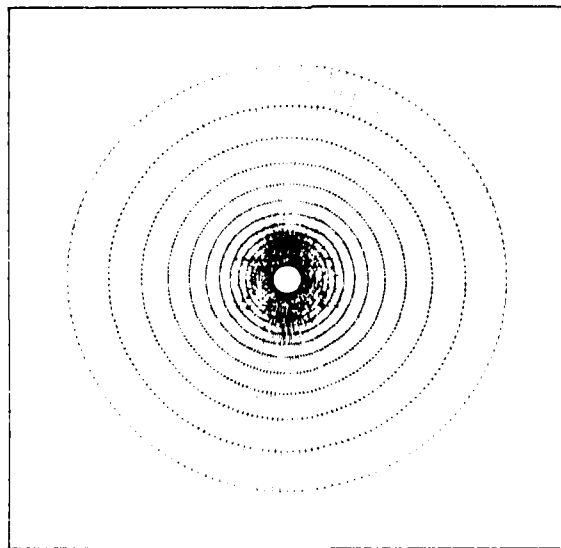
The complex flow field is established when a shock wave strikes an object with features such as reflected shocks and Mach stems. To verify that the code can predict such flows, the interaction of a shock travelling past a cylinder was studied. Both inviscid and turbulent-viscous flows were calculated to illustrate any differences in the flow due to turbulent-viscous effects.

Inviscid calculations of this problem have been performed by both Gatter and Fernquist² and Mark and Kutler.¹⁵ It is important to keep in mind that the inviscid flow over a half-cylinder on a flat surface (the field structure case for this work) is identical to the inviscid flow over a "free standing" cylinder. Thus the inviscid shock-cylinder flow represents both a test case and case to compare with the flow over a half-cylinder on a surface.

An analytically described mesh in a cylindrical coordinate system was employed for the shock-cylinder interaction flow as shown in Figure 3-7. The grid is determined by the cylinder body radius, the distance from the body to the outer boundary, and the distance from the body and the first point away from the body. Rays were equally spaced around the body, and points along rays were radially clustered near the body by an exponential function. The



a) Inviscid flow grid



b) Viscous flow grid

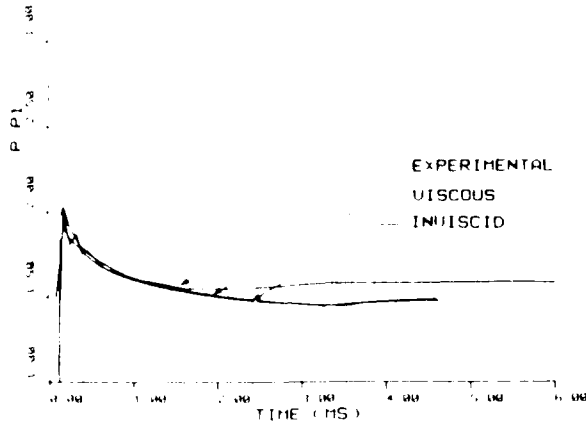
Figure 3-7. Grids used in shock-cylinder interaction calculation

two grids shown in Figure 3-7 differ in that the turbulent viscous flow grid has a larger number of grid points along the rays away from the body with a smaller distance from the body to the first grid point. The details of the grids are given in Table 3-1.

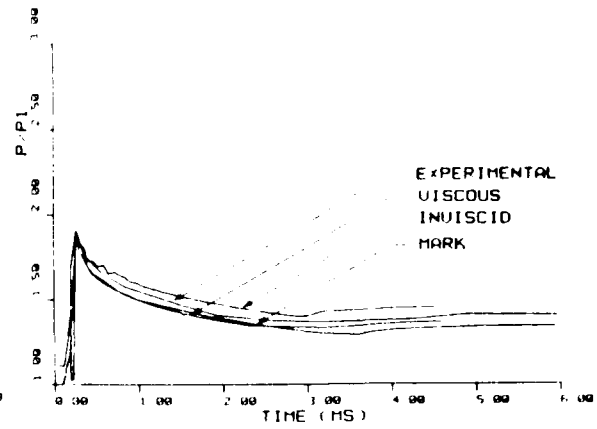
3.2.1 Results

The conditions chosen for the cylinder flows were designed to match the experimental conditions of Pearson, et al.,¹⁵ at the Ballistic Research Laboratory. In their work a 0.305m diameter aluminum cylinder was rigidly fixed across a 2.44m diameter shock tube. A flattop shock wave with an overpressure of 42 kPa (6.09 psi) passed over the cylinder. Ambient (preshock) pressure for this experiment was 101.3 kPa (14.69 psi) with an ambient density of 1.22 kg/m³. These calculations were done with a constant wall temperature for the viscous flow. The Reynold number based upon the cylinder diameter is 6.95×10^6 .

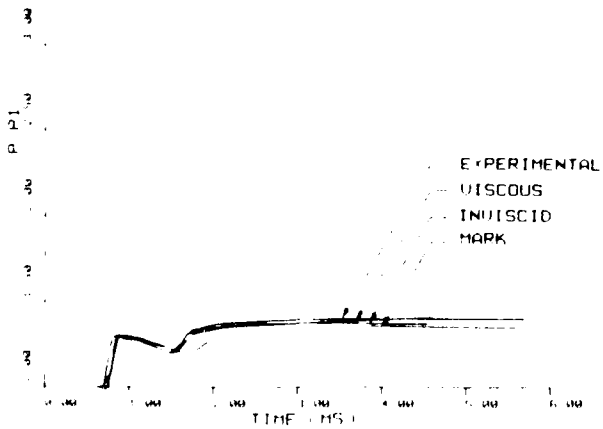
In many respects, the results of the inviscid and turbulent-viscous runs are quite similar. Figure 3-8 compares predicted pressure-time histories at several locations on the cylinder ($\theta = 0, 45, 135, 180$) with those experimentally measured, and with the inviscid calculations of Mark and Butler. (The experimental data presented are an average of the actual measurements which contained substantial high frequency oscillations.) The sharp rise in pressure at each location signifies the arrival of the shock. The pressure at all stations, except 180°, then decreases until it "jumps" again and then reaches a plateau level. This second jump is the result of a reflected shock which is created at the rear of the cylinder and propagates upstream over the cylinder, as illustrated by the isopycnics of Figures 3-9 and 3-10.



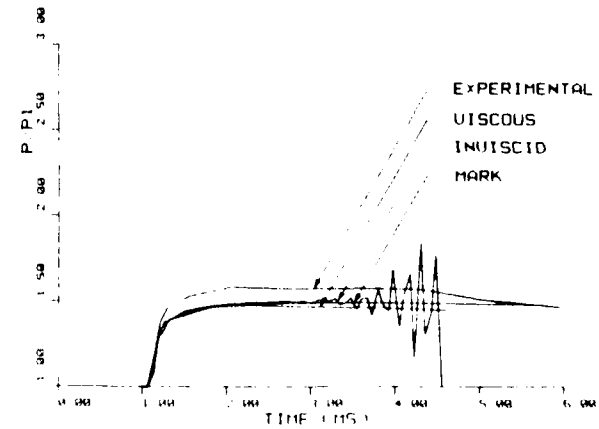
a) $\theta = 0^\circ$



b) $\theta = 45^\circ$

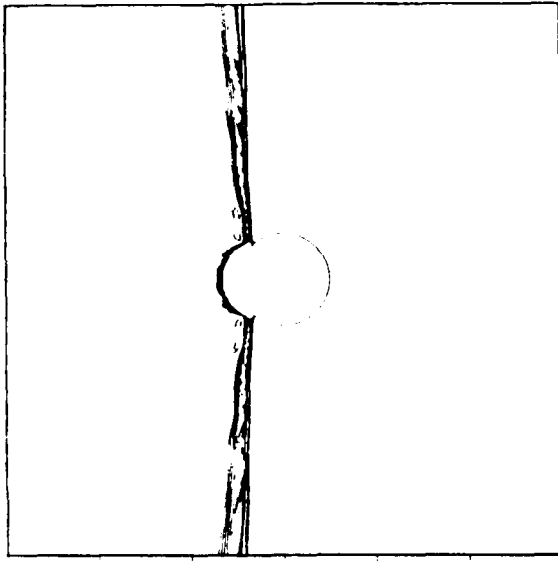


c) $\theta = 135^\circ$

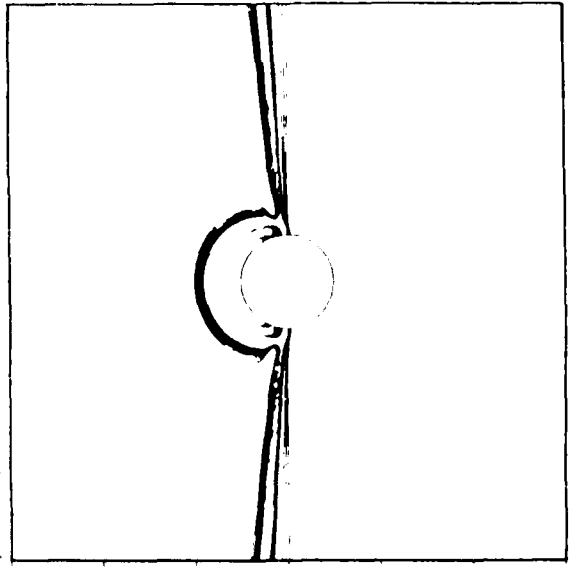


d) $\theta = 180^\circ$

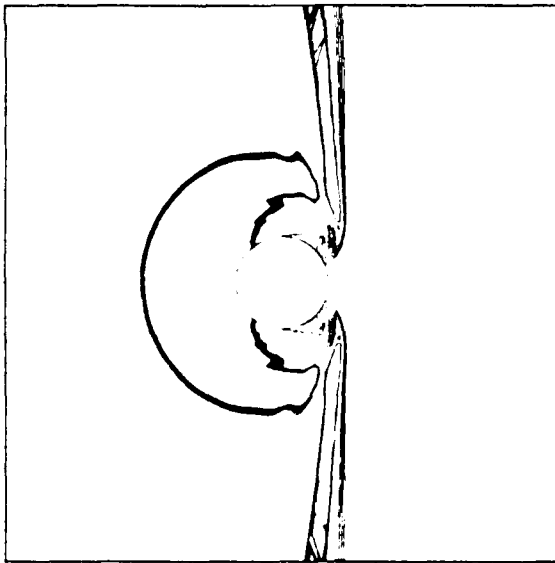
Figure 3-8. Pressure-time histories for shock-cylinder interaction



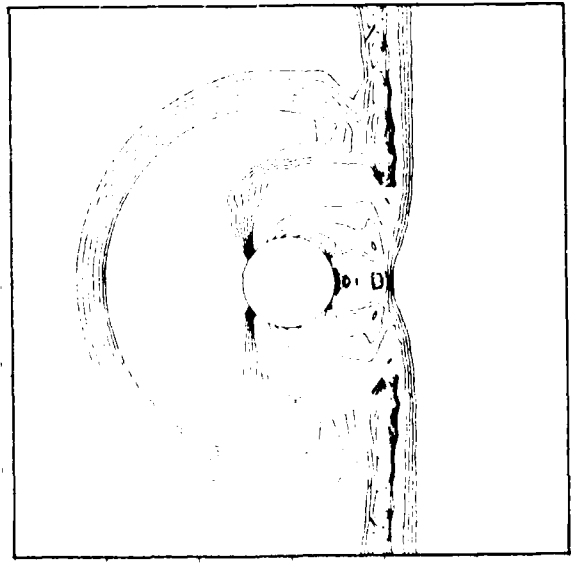
a) 0.25 ms



b) 0.50 ms

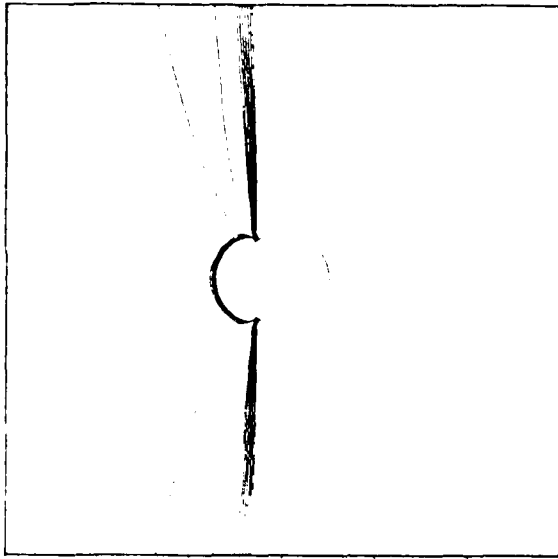


c) 1.01 ms

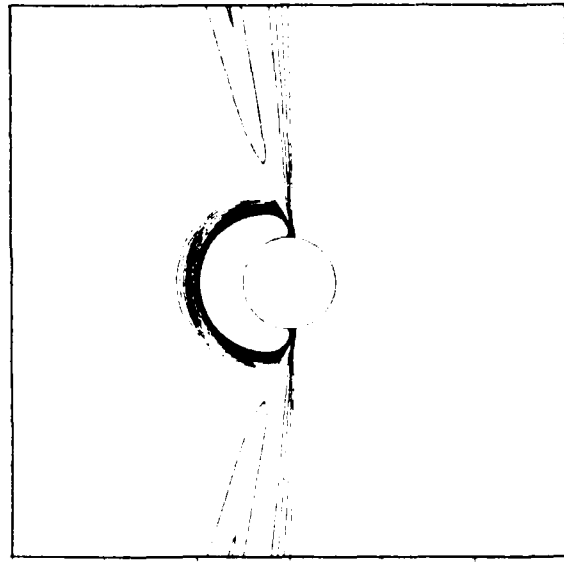


d) 1.52 ms

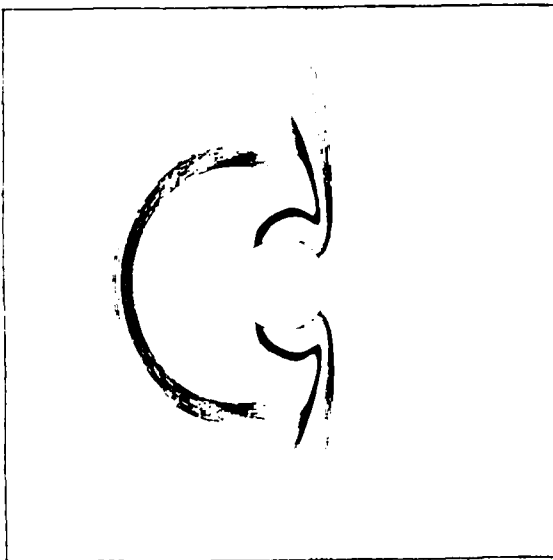
Figure 3-9. Computed inviscid isopycnics of shock-cylinder interaction at various times



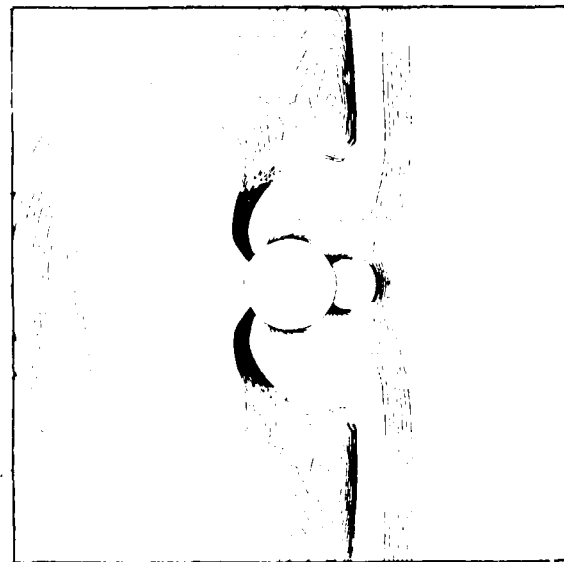
a) 0.25 ms



b) 0.40 ms



c) 0.85 ms



d) 1.35 ms

Figure 3-10. Computed turbulent-viscous isopycnics of shock-cylinder interaction at various times

These figures illustrate some interesting features of the computations. First note that the shock is increasingly "smeared" far from the cylinder. This is a result of the grids. From Figure 3-7, it is obvious that the circumferential grid spacing increases with distance from the cylinder. Thus the coarse grid results in poor resolution of the shock. Secondly, the isopycnics of the viscous flow are much sharper than those of the inviscid calculation. This is a result of the finer mesh of the grid used the viscous calculation. In addition, the increased damping of the viscous terms smooths the isopycnics.

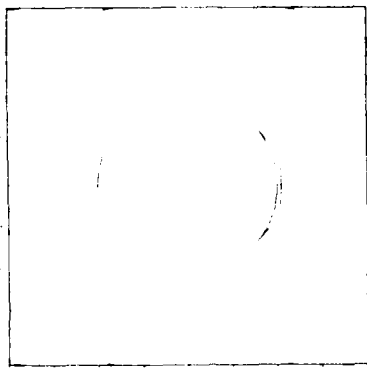
Noticeable differences between the experimental data and the calculations in the time-pressure histories exist at the stagnation point (0°) and at 180° . One difference is that the plateau level of the viscous calculation of $p/p_1 = 1.49$ is closer to the steady state stagnation pressure ratio of 1.46 than is the experimental value of 1.59. This occurs at a time when there is a possibility of reflections from the walls of the shock tube affecting the measured pressure. Therefore, we have some reservations about the interpretation of the data.

Another possible source of the discrepancy at 180° could be the distortion of the cylinder during the experiment. The object of the experimental study was to determine the buffet on generic aircraft structures. Thus, the cylinder wall was thin aluminum and posttest inspection showed that the cylinder was deformed. Therefore, it is possible that the cylinder deformed enough during the passage of the shock to affect the flowfield.

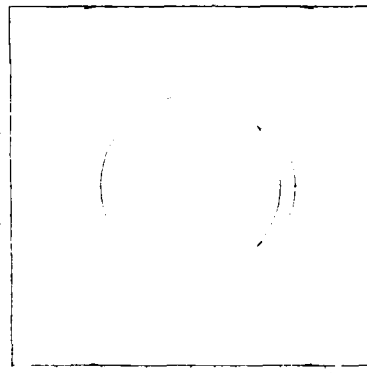
Figure 3-8d shows a growing temporal oscillation in the predicted inviscid pressure at the 180° location. The source of this instability in the

inviscid calculation is unknown. When viscosity was "turned on" it disappeared and therefore was not investigated further.

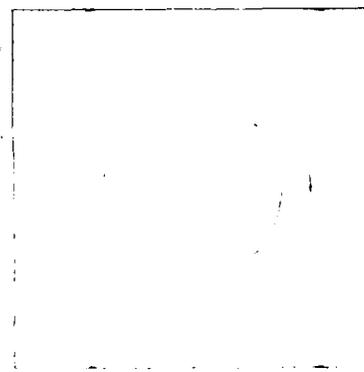
An important point with regard to the turbulent viscous calculation is the grid spacing at the cylinder surface. Even though our flat plate studies suggest a minimum spacing on the order of 10^{-6} , computation time requirements precluded using a grid with so fine a spacing. The minimum spacing of the cylinder grid ($\Delta r/d$) is 8×10^{-5} . With this grid, 140,000 steps are required for this flow calculation using 11 hr on the CRAY X-MP computer. Thus, while the primary features of the flow appear correct, the magnitude of the friction component of the drag cannot be expected to be correct. Still, the calculated flow does separate from the rear of the cylinder. Figure 3-11 shows the development of the separation bubble behind the cylinder. The bubble was still growing when the calculation was stopped. For comparison the stream function contours of the inviscid calculation are shown in Figure 3-12. As the study of steady flows is not the main objective of this work, both the viscous and inviscid calculations were stopped before steady state conditions were obtained.



a) 2.9 ms



b) 3.6 ms



c) 4.7 ms

Figure 3-11. Development of separation bubble behind cylinder in turbulent viscous flow of shock-cylinder interaction calculation.

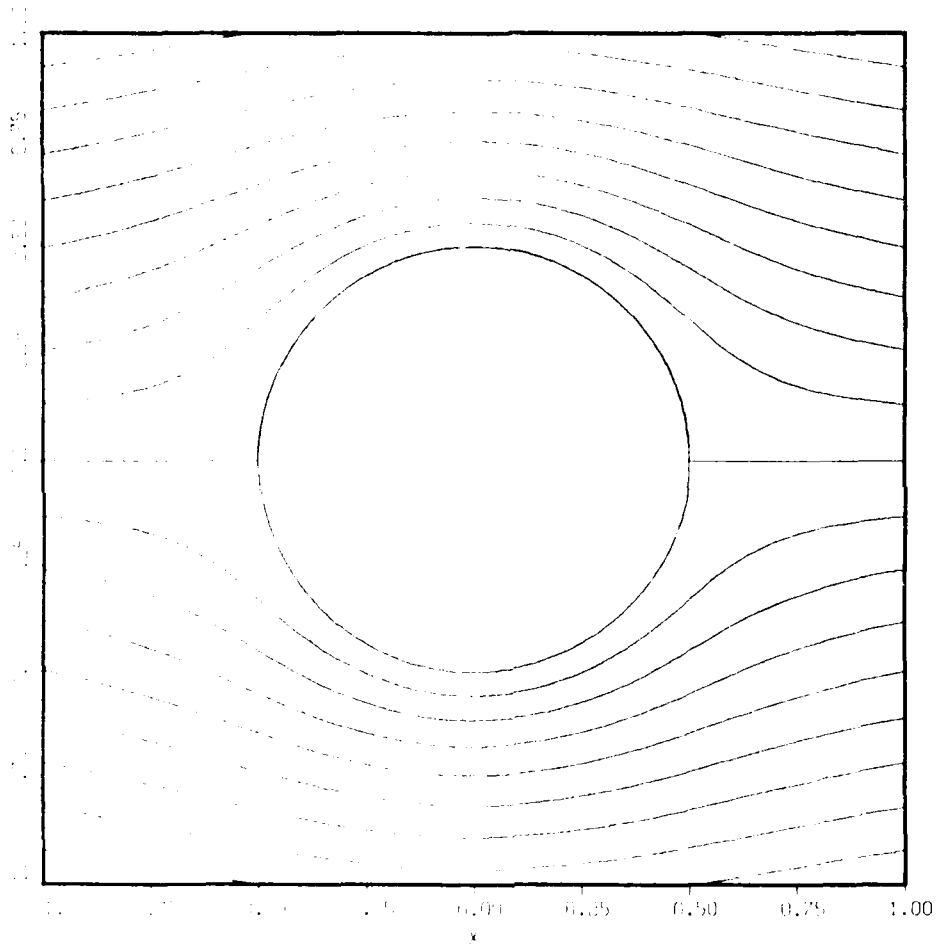


Figure 3-12. Calculated inviscid stream function contours of shock cylinder interaction at 4.2 ms

SECTION 4

SHOCK STRUCTURE FLOWFIELD

4.1 PROBLEM DESCRIPTION

The final study of this work is a calculation of the flow behind a blast wave passing over an object on the earth's surface. It has a number of features which are combinations of those in the other test cases; a shock wave moving past a cylinder and a boundary layer on a flat surface. We chose a 2 m radius half-cylinder geometry to model this problem. A consideration of some other physical parameters reveals interesting information, as described below.

At a distance of 2000m from a 1 megaton explosion, the resulting blast wave has approximately a 172 kPa (25 psi) overpressure ($M_S = 1.58$). In order to numerically resolve the turbulent boundary layer which forms behind the blast wave, the grid needs at least a few points in the viscous sublayer (as discussed in Section 3.1). At 10m behind such a blast wave, the turbulent boundary layer is less than 10 cm high. Thus, as previously discussed, grid spacing on the order of 10^{-6} m is required. For a calculation which is time accurate, i.e., to satisfy the CFL condition, this translates into approximately 10^7 time steps for the early time interaction with an object. Such a calculation would require over 150 hr on the CRAY X-MP. For this present work, this amount of computational time is unacceptable. Therefore, the calculation is done with a coarser grid so that time accurate

Calculations can be made with a reasonable amount of computer resources. Based on the test case results, the results should be valid for evaluating global flowfield effects, but skin friction and heat transfer calculations are not expected to be accurate.

Several quasi-steady state calculations were attempted to supplement the time accurate calculation. These runs included a boundary layer profile in the inflow boundary conditions. The thickness of these profiles was on the order of the height of the cylinder, thus modeling conditions when the shock is far downstream of the protruding cylinder. These calculations are not limited by the small step size requirements of time accurate calculations, and therefore include the fine mesh required for accurate resolution of viscous effects.

Unfortunately, these quasi-steady calculations failed to converge. Our studies indicate that this lack of convergence is due to either the boundary conditions or the grid (especially the large aspect ratio of some cells, a result of computer limitations). However, we do not yet have a definitive answer to the question.

1.2. Grid

The grid used in the time-accurate calculations was generated with a hyperbolic grid generator developed at NASA Ames Research Center.⁶ This grid generator produces a grid which is orthogonal to the wall, while allowing a change of the first grid space. The stretching away from the wall is exponential. The grid developed for the time accurate calculations is shown in Figure 4-1.

1.3. Results

A calculation was performed for a shock with a pressure ratio of 2.75 moving over an arched structure (half cylinder) on a wall (i.e., the ground).

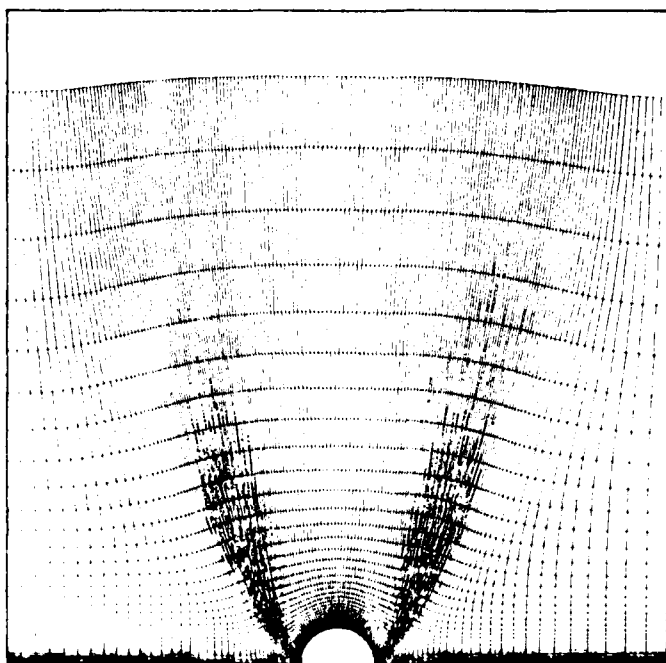


Figure 4-1. Grid used for shock field structure flow

The calculation continued until the shock reached the downstream grid boundary which was seven cylinder radii downstream from the cylinder. A calculation similar to this was performed by Kurylo et al.¹⁶ Their flow configuration consisted of a shock wave with a 1.33 pressure ratio passing an arched structure with a height-to-width ratio of 1.3. The calculations of Kurylo¹⁶ were performed on a very coarse grid and were stated to have been carried out to "steady state." However, no intermediate time results were presented, and we suspect their grid is too coarse to resolve the viscous layers in the flow. We will note the differences between their results and ours below.

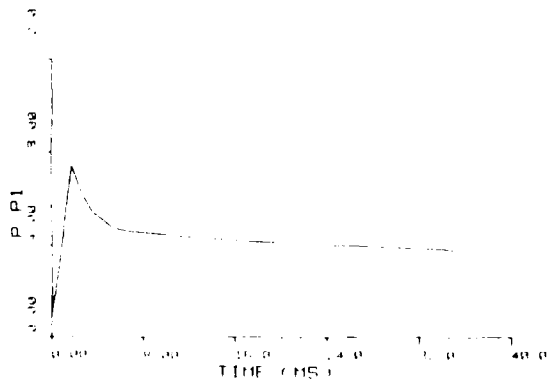
The results of the present calculation are presented in several ways. Pressure-time histories at different locations on the cylinder are given

in Figure 4-2. The locations are identical to those plotted for the shock-cylinder interaction. Although the shock is much stronger in this case, the structure of the pressure-time histories is similar to the cylinder results. The shock structure at various times is shown by isopycnics in Figure 4-3. Again the flowfield structure is similar to that of the flow without the wall. Also note that the shock does not become more "smeared" away from the wall. This result is because the grid spacing does not increase in the streamwise direction as it did for the grids used in the shock-cylinder calculation. A distinguishing feature of this flow is the gradual drop in pressure which is shown in Figure 4-2 ($\theta = 180^\circ$) at $t \sim 20$ ms. This drop in pressure corresponds to the development of the separated flow as shown in Figure 4-4.

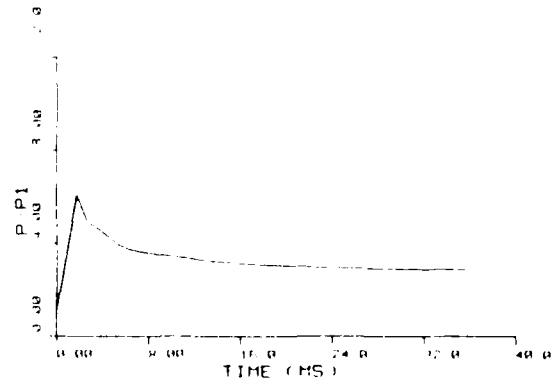
As with the viscous flow over the free-standing cylinder, a region of separated flow also develops behind the half cylinder. In this case the curvature of the wall accelerates the growth of the region. Here the difference of the flow from the inviscid solution is obvious.

Another feature which is perhaps more interesting accentuates the effect of the viscous wall flow on the flowfield. Figure 4-5 shows the development of a separated flow region in front of the structure. This feature was not found in the calculations of Kurylo, perhaps due to the smaller height-to-width ratio of their structure. By the time the shock is only 4 diameters past the half-cylinder the height of the separated region is nearly 20 percent of the structure height.

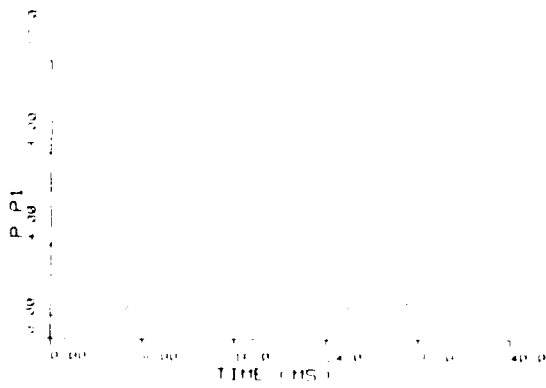
In summary, the inclusion of viscous-turbulent effects significantly changes the flow over a half cylinder on a surface. The effects of viscosity are apparent despite the need for a coarse grid, which can not be expected to accurately resolve the boundary layer near a wall.



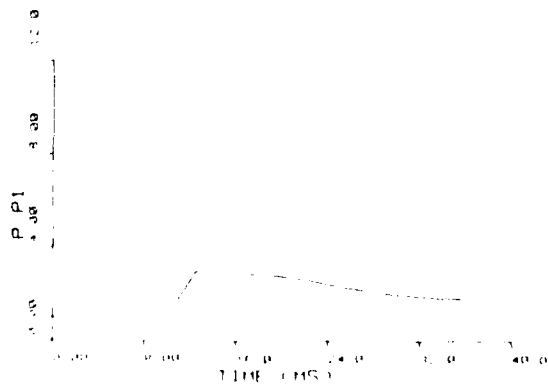
a) $\theta = 0^\circ$



b) $\theta = 45^\circ$

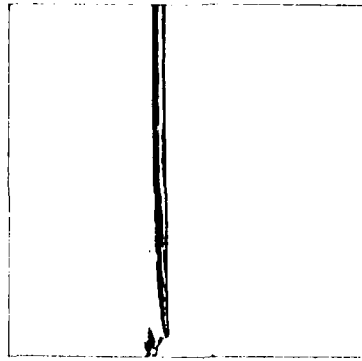


c) $\theta = 135^\circ$

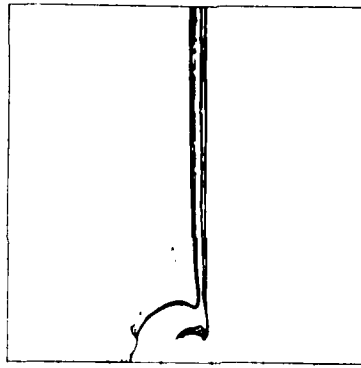


d) $\theta = 180^\circ$

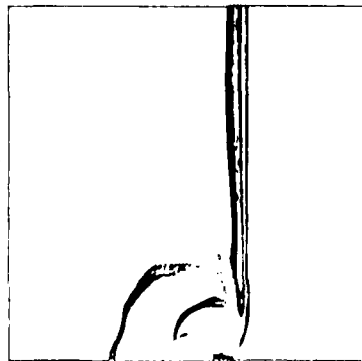
Figure 4-2. Calculated pressure-time histories for shock-field structure interaction



a) 1.79 ms

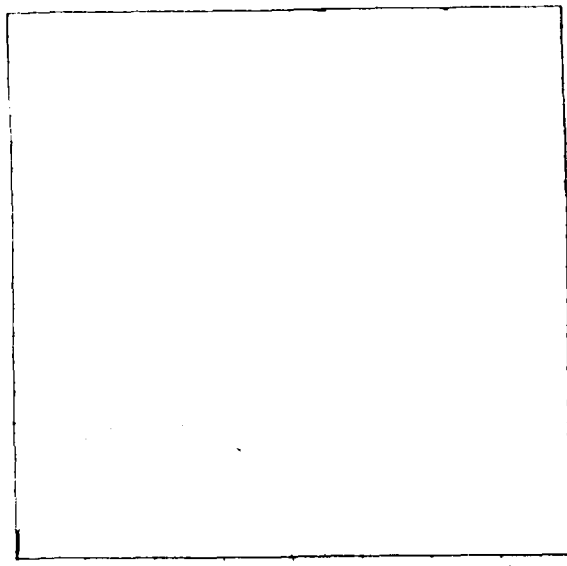


b) 7.16 ms

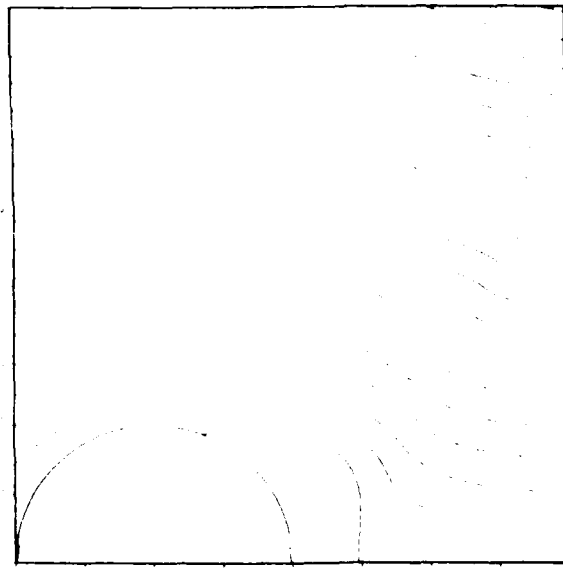


c) 12.50 ms

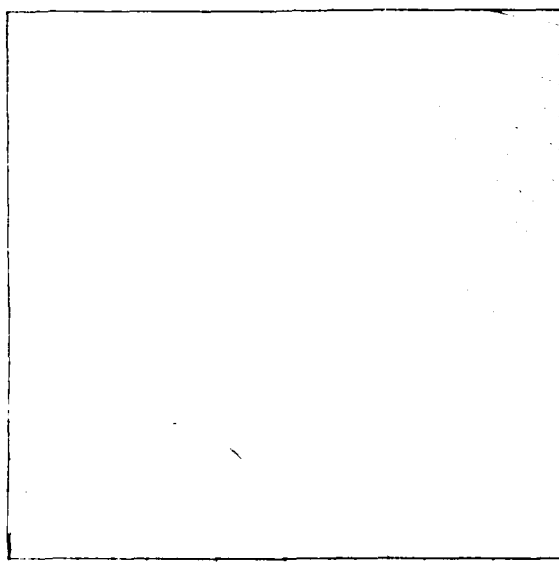
Figure 4-3. Computed turbulent-viscous isopycnics of shock-field structure interaction at various times



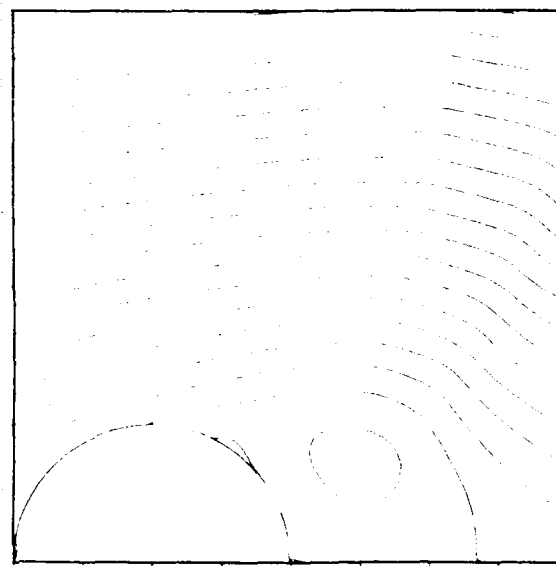
a) 19.6 ms



b) 24.1 ms

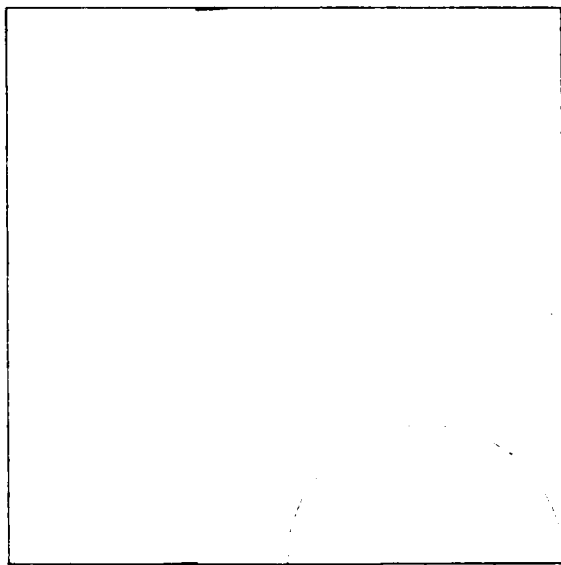


c) 27.7 ms

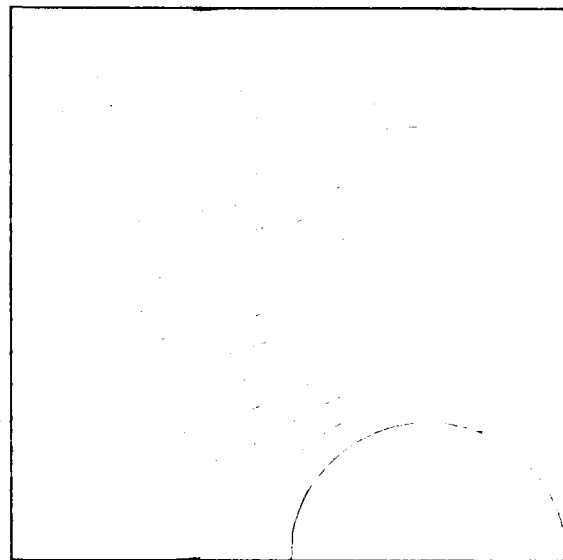


d) 35.7 ms

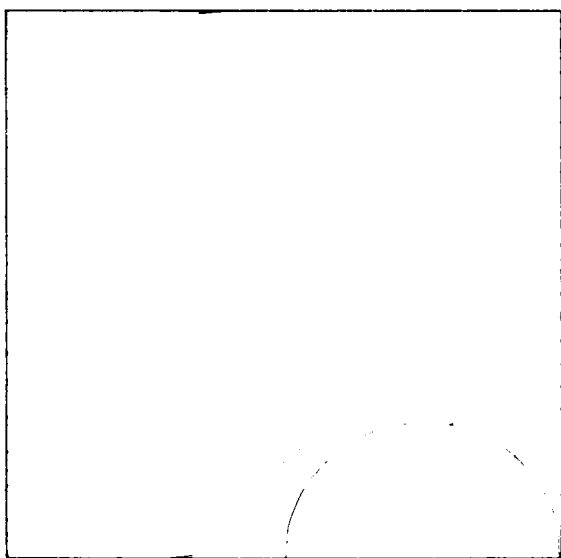
Figure 4-4. Stream function contours showing development of separated flow at rear of structure



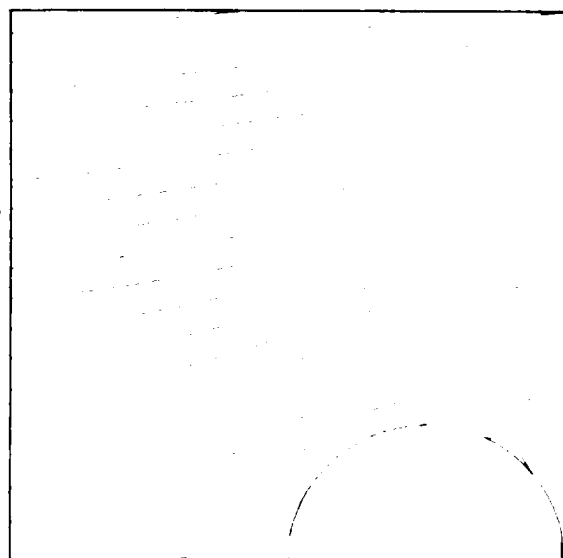
a) 19.6 ms



b) 24.1 ms



c) 27.7 ms



d) 35.7 ms

Figure 4-5. Stream function contours showing development of separated flow in front of structure

SECTION 5

SUMMARY AND CONCLUSIONS

The flow resulting from the interaction of a planar shock wave and an object on the ground was calculated with the full Navier-Stokes equations, including turbulence effects. The resulting flowfields show the development of regions of separation both before and aft of the structure, thus illustrating the importance of including turbulence and viscous effects in predicting flowfields resulting from blast waves passing over structures. These results suffer from a need to use a coarse grid that can not adequately resolve the details of the boundary layer wall region. The use of a finer grid was not feasible due to the inordinately long computing times which would result, even on the CRAY X-MP computer.

Test cases verified that the implicit finite difference code, ARC2D, could accurately predict boundary layer phenomena and shock-object interaction given a sufficiently fine grid. Still the code does have its limitations and more effort is required to solve the quasi-steady flow over the structure on a wall (part of this effort would probably be an improved grid).

Improvements in several areas would greatly increase the accuracy of future turbulent-viscous flow calculations. First, the addition of some scheme to the code to reduce pressure overshoot and the resulting oscillations would be of benefit. Second order dissipation near a shock has been added to ARC2D for time asymptotic calculations and its implementation for time

accurate calculations should be forthcoming. This should be applied to the present cases. Additionally, validated methods for calculating separated turbulent boundary layers with a course grid would be helpful (perhaps something like a "wall function" for separated flow).

REFERENCES

1. Abbett, M. J., L. Cooper, T. J. Dahm, and M. D. Jackson, "PANT Interim Report, Volume IX, "Unsteady Flow on Ablated Nosed Tip Shapes -- PANT Series G Test and Analysis Report," SAMS0-TR-74-86, December 1973.
2. Kutler, P. and A. Fernquist, "Computation of Blast Wave Encounter with Military Targets," Flow Simulations, inc., Report No. 80-02, April 30, 1980.
3. Pulliam, T. H., "Euler and Thin Layer Navier -- Stokes Codes: ARC2D, ARC3D." Notes for Computational Fluid Dynamics User's Workshop, University of Tennessee Space Institute, March 1984.
4. Pulliam, T. H. and J. L. Steger, "Recent Improvements in Efficiency, Accuracy, and Convergence for Implicit Approximate Factorization Algorithms," AIAA paper AIAA-85-0360, AIAA 23rd Aerospace Sciences Meeting, 1984.
5. Barth, T. J. and T. H. Pulliam, "Navier-Stokes Computations for Exotic Airfoils," AIAA paper AIAA-85-0109, AIAA 23rd Aerospace Sciences Meeting, 1984.
6. Barton, J. T. and T. H. Pulliam, "Airfoil Computation at High Angles of Attack, Inviscid and Viscous Phenomena," AIAA paper 84-0524, AIAA 22nd Aerospace Science Meeting, Reno Nevada, 1984.
7. Beam, R. and R. F. Warming, "An Implicit Finite-Difference Algorithm for Hyperbolic Systems in Conservation Law Form," J. Comp. Phys. 22, 87-110, 1976.
8. Baldwin, B. S. and H. Lomax, "Thin Layer Approximation and Algebraic Model for Separated Turbulent Flows," AIAA paper no. 78-257, 1978.
9. Mirels, H., "Boundary Layer Behind a Shock or Thin Expansion Wave Moving Into a Stationary Fluid," NACA TN3712, May 1956.
10. Hartunian, R. A., A. L. Russo, and P. V. Morrone, "Boundary Layer Transition and Heat Transfer in Shock Tubes," Journal of the Aerospace Sciences, August 1960.
11. Pulliam, T. H., "Artificial Dissipation Models for the Euler Equations, AIAA Paper, AIAA-85-0438, January 1985.
12. Martin, W. A., "An Experimental Study of the Turbulent Boundary Layer Behind the Initial Shock Wave in a Shock Tube," Journal of the Aerospace Sciences, October 1958.
13. Martin, W. A., "An Experimental Study of the Boundary Layer Behind a Moving Plane Shock Wave, University of Toronto Institute of Aerophysics Report No. 47, May 1957.

14. Mark, A. and P. Kutler, "Computation of Shock Wave/Target Interaction," AIAA paper AIAA-83-0039, January 1983.
15. Pearson, R. J., H. L. Wisniewski, and P. D. Szabados, "Synergism in Nuclear Thermal/Blast Loading," Proceedings of the 7th International Symposium on Military Application of Blast Simulation, Ralston, Alberta, Canada, July 1981.
16. Kurylo, J, S. Hancock, and Y. Kivity, "Viscous Flow Calculations of Shock Diffraction and Drag Loads on Arched Structures," AIAA paper AIAA-84-1680, June 1984.

END

FILMED

5-85

DTIC